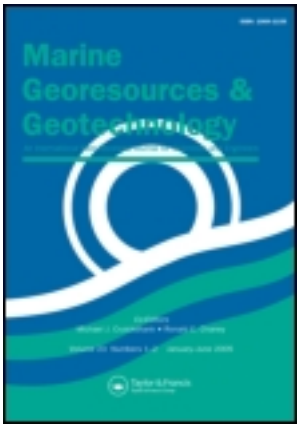

Marine Georesources & Geotechnology
Publication details, including instructions for authors and subscription information:
http://www.tandfonline.com/loi/umgt20

Deep-sea Fe-Mn Crusts from the Northeast Atlantic Ocean: Composition and Resource Considerations

Susana Bolhão Muiños [a c], James R. Hein [b], Martin Frank [c], José Hipólito Monteiro [a], Luís Gaspar [a], Tracey Conrad [b], Henrique Garcia Pereira [d] & Fátima Abrantes [a]

[a] Unidade de Gelogia Marinha, Laboratório Nacional de Energia e Geologia, Amadora, Portugal

[b] U.S. Geological Survey, Santa Cruz, CA, USA

[c] GEOMAR, Helmholtz Centre for Ocean Sciences, Kiel, Germany

[d] CERENA, Instituto Superior Técnico, Universidade Técnica de Lisboa, Lisboa, Portugal

Version of record first published: 18 Jan 2013.

To cite this article: Susana Bolhão Muiños , James R. Hein , Martin Frank , José Hipólito Monteiro , Luís Gaspar , Tracey Conrad , Henrique Garcia Pereira & Fátima Abrantes (2013): Deep-sea Fe-Mn Crusts from the Northeast Atlantic Ocean: Composition and Resource Considerations, Marine Georesources & Geotechnology, 31:1, 40-70

To link to this article: http://dx.doi.org/10.1080/1064119X.2012.661215

Marine Georesources & Geotechnology, 31:40–70, 2013

ISSN: 1064-119X print/1521-0618 online
DOI: 10.1080/1064119X.2012.661215

Taylor & Francis
Taylor & Francis Group

Deep-sea Fe-Mn Crusts from the Northeast Atlantic Ocean: Composition and Resource Considerations

SUSANA BOLHÃO MUIÑOS*[1,3], JAMES R. HEIN[2], MARTIN FRANK[3], JOSÉ HIPÓLITO MONTEIRO[1], LUÍS GASPAR[1], TRACEY CONRAD[2], HENRIQUE GARCIA PEREIRA[4], AND FÁTIMA ABRANTES*[1]

[1]Unidade de Gelogia Marinha, Laboratório Nacional de Energia e Geologia, Amadora, Portugal
[2]U.S. Geological Survey, Santa Cruz, CA, USA
[3]GEOMAR, Helmholtz Centre for Ocean Sciences, Kiel, Germany
[4]CERENA, Instituto Superior Técnico, Universidade Técnica de Lisboa, Lisboa, Portugal

Eighteen deep-sea ferromanganese crusts (Fe-Mn crusts) from 10 seamounts in the northeast Atlantic were studied. Samples were recovered from water depths of ~1,200 to ~4,600 m from seamounts near Madeira, the Canary and Azores islands, and one sample from the western Mediterranean Sea.

The mineralogical and chemical compositions of the samples indicate that the crusts are typical continental margin, hydrogenetic Fe-Mn crusts. The Fe-Mn crusts exhibit a Co + Cu + Ni maximum of 0.96 wt%. Platinum-group element contents analyzed for five samples showed Pt contents from 153 to 512 ppb.

The resource potential of Fe-Mn crusts within and adjacent to the Portuguese Exclusive Economic Zone (EEZ) is evaluated to be comparable to that of crusts in the central Pacific, indicating that these Atlantic deposits may be an important future resource.

Received 1 July 2011; accepted 29 December 2011.

We thank the Portuguese Science and Technology Foundation (FCT) for financial support through Project PDCT/MAR/56823/2004; FCT also supported a fellowship to S.B.M. (SFRH/BD/22263/2005) co-financed by POCI 2010/EU. Additional support to S.B.M. was provided by a LNEG fellowship. We acknowledge K. Hoernle, the crew and scientific party of Meteor M51/1 cruise as well as the Deutsche Forschungsgemeinschaft (DFG, German Research Council) for funding. We acknowledge J. Girardeau, the onboard scientific team, the University of Nantes and the French INSU-CNRS Institute for the financial support that made possible the collection of the samples from the Tore-Madeira Cruise and for kindly having made these samples available for this work. We also thank the co-chiefs of the TTR-11 Cruise, the onboard team and the UNESCO–IOC TTR Program for the samples collected during the TTR-11 cruise, which was funded by INGMAR Project (FCT). We also thank S. M. Lebreiro, L. M. Pinheiro, R. Dunham, J. Noiva, J. Dias, F. Neves, C. Lopes and M. Mil-Homens for their help and discussions. The editors and two anonymous reviewers are thanked for their contribution to the improvement of this paper.

*Current affiliation: Divisão de Geologia e Georecursos Marinhos, Instituto Português do Mare e da Atmosfera, Lisboa, Portugal.

Address correspondence to Susana Bolhão Muiños, Instituto Português do Mar e da Atmosfera, I.P., Divisão de Geologia e Georecursos Marinhos, Rua C-Aeroporto de Lisboa, 1749-077 Lisboa, Portugal. E-mail: susana.muinos@ipma.pt

Keywords ferromanganese crusts, northeast Atlantic, Portuguese EEZ, resource considerations, seamounts

Introduction

Manganese and ferromanganese oxide deposits in the oceans occur as nodules, crusts, and massive beds. These deposits have been classified as diagenetic, hydrogenetic, hydrothermal, and mixed-type deposits (Halbach 1986; Hein et al. 1997; Wen et al. 1997). Hydrogenetic crusts (Fe-Mn crusts) form by direct precipitation of colloidal hydrated metal oxides from the water column onto hard-rock substrates.

The first investigations of hydrogenetic Fe-Mn crusts on seamounts were carried out in the Pacific Ocean (Craig et al. 1982; Halbach et al. 1982, 1989b; Hein et al. 1988). The preconditions required for Fe-Mn crust formation, such as the occurrence of isolated volcanic edifices, strong currents that keep the edifices free of sediment, and an oxygen-minimum zone (OMZ) are also found in the Atlantic Ocean (Koschinsky et al. 1995). Indeed, previous results from NE Atlantic seamounts indicate widespread presence of Fe-Mn crusts of hydrogenetic origin (Koschinsky et al. 1995, 1996; Gaspar 2001; Muiños et al. 2002; Muiños 2005). Hydrogenetic precipitation is dependent on water-mass properties and is characterized by slow growth rates (< 10 mm/Ma) and generation of an extremely high specific-surface area, which promotes the enrichment of trace elements through scavenging by the major oxides (e.g., Hein et al. 1997). Seamounts act as obstructions to oceanic water-mass flow thereby creating seamount-generated currents of enhanced energy relative to flows away from the seamounts. These currents, which are strongest along the outer rim of the summit region of seamounts, promote the formation of thick crusts, enhanced turbulent mixing, and produce upwelling, leading to increased primary productivity and thus maintenance of the OMZ (summarized in Hein et al. 2000). Manganese oxides and associated trace metals are concentrated in the OMZ, which are then scavenged onto crusts under oxic conditions resulting from the turbulent mixing around seamounts.

Our study area in the northeast Atlantic (Figure 1) is influenced by the Mediterranean Outflow Water (MOW), which is characterized by relatively high salinity and temperature and low oxygen content compared to surrounding water masses. Because manganese is soluble under low-oxygen conditions, this water mass is a reservoir for Mn^{2+} in solution between 800 and 1,200 m water depth, which corresponds to the upper and lower cores of the MOW (Madelain 1970; Zenk 1970; Ambar and Howe 1979; Ambar et al. 1999, 2002). Fluctuations in the intensity of the OMZ and MOW may have influenced the composition of the Fe-Mn crusts (Koschinsky et al. 1996).

Hydrogenetic precipitation promotes the enrichment of crusts in potentially economically important trace metals such as Co, Ni, Te, rare earth elements (REEs), and platinum-group elements (PGEs), and thus there is a growing recognition of Fe-Mn crusts as potential metal resources. With growing markets for metals in Asia, as well as the rapid development of high-tech and green-tech applications, the demand for rare earth metals will increase dramatically in the near future (Hein et al. 2010).

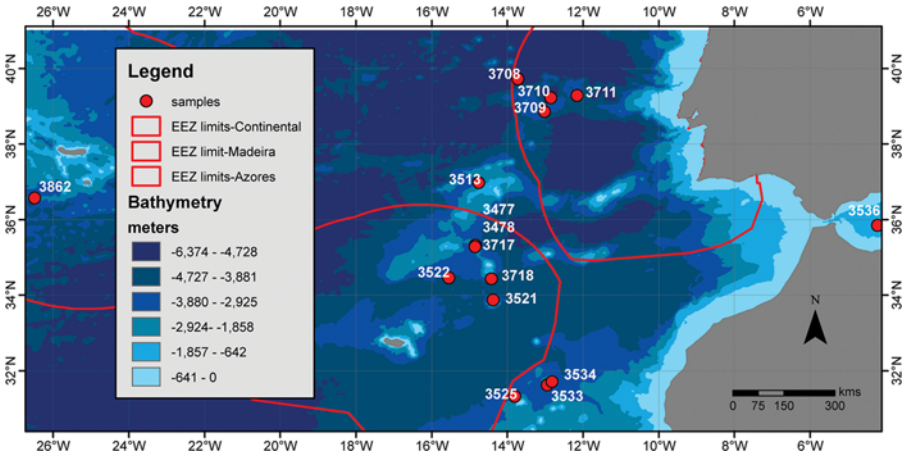

Figure 1. Map showing bathymetry, the location of the sample sites, and the limits of the Portuguese EEZ. (Color figure available online.)

Significantly, to our knowledge, there is a lack of technology needed for detailed exploration and extraction of Fe-Mn crusts, which may be slowing development. However, much proprietary engineering research has been undertaken in a number of countries. Environmental studies are also in their infancy and should be addressed as stipulated in the United Nations Convention on the Law of the Sea and International Seabed Authority regulations. Accompanying the accelerating economic interest in Fe-Mn crusts, the International Seabed Authority passed regulations for exploration for Fe-Mn crusts during its 18th Session in July 2012.

Much work has been done on marine Fe-Mn deposits, but studies of Atlantic Ocean deposits are still scarce compared to those from the Pacific Ocean. The aims of this study are to determine the composition of Fe-Mn crusts from the northeast Atlantic, in particular those within the Portuguese Exclusive Economic Zone (EEZ), and to consider their resource potential.

Material and Methods

Samples were collected from 10 seamounts in the northeast Atlantic during cruises Trident 86, TTR-11 (I.O.C. 2002), Meteor 51/1 (Hoernle and Scientific Party 2003), and Tore-Madeira (Merle 2006). Sampling occurred over a wide geographic range including seamounts in the Portuguese EEZ and near the Canary Islands. Sampling locations are distributed over a large depth range and the growth and composition of the Fe-Mn crusts were influenced by different chemical and oceanographic environments that are broadly representative of the study area (Figure 1 and Table 1).

The chemical and mineralogical data represent analyses of bulk samples. All crusts were analyzed by X-ray diffraction on a Philips diffractometer using Cu-Kα radiation and carbon monochromator at the United States Geological Survey (USGS). The interpretation of the diffractograms and identification of mineralogical phases were also performed at the USGS using the program X'Pert High Score of Philips (PANalytical). We follow the nomenclature of Usui et al. (1989) for manganese minerals. The semi-quantitative determination of mineral content is based on

Table 1. Location of samples

Sample ID	Field ID	Latitude (N)*[1]	Longitude (W)*[1]	Water Depth (m)*[1]	Seamount	Geographic Area
3477-B.3.4	TTR11-353GR	35.3117	−14.8300	1853	Nameless	Madeira
3478-B.3.5	TTR11-354GR	35.3167	−14.8350	1839	Nameless	Madeira
3717-12	TM-D19	35.2767	−14.8500	2198	Nameless	Madeira
3521-6	M51/1-426DR	33.8683	−14.3680	1362	Seine	Madeira
3522-4	M51/1-428DR	34.4567	−15.5387	2946	Godzilla	Madeira
3718-1	TM-D20	34.4258	−14.4173	3756	Unicorn	Madeira
3513-13	M51/1-414DR	36.9700	−14.7475	4594	MTR-Josephine	Madeira
3513-14	M51/1-414DR	36.9700	−14.7475	4594	MTR-Josephine	Madeira
3513-16	M51/1-414DR	36.9700	−14.7475	4594	MTR-Josephine	Madeira
3708-1	TM-D3B	39.7217	−13.7152	4140	Tore	Madeira
3709-1	TM-D5	38.8442	−13.0147	2803	Tore	Madeira
3710-1	TM-D6B	39.2158	−12.8464	4245	Tore	Madeira
3711-2	TM-D9	39.2775	−12.1486	3110	Tore	Madeira
3525-9	M51/1-448DR	31.3216	−13.8009	3043	Dacia	Canaries
3533-7	M51/1-457DR	31.6267	−12.9382	1602	Annika	Canaries
3534-14.1	M51/1-458DR	31.7083	−12.8156	2128	Annika	Canaries
3536-3	M51/1-462DR	35.8450	−4.2125	1221	Ibn Batouta	Mediterranean
3862	TR86-8D	36.5667	−26.4833	2575	Azores	Azores

*[1]Except for samples from the TTR-11 cruise that were collected by TV-Grab, all the other coordinates and water depths (M51/1- Meteor 51/1, TM-Tore-Madeira and TR-Trident 86) correspond to intermediate values from on- and off-bottom dredge locations. MTR means Madeira-Tore Rise.

the relative intensity of the peaks and previously determined weighing factors (Cook et al. 1975; Hein et al. 1988).

Major elements (Fe, Mn, Si, Al, Ca, Mg, Na, K, Ti, P) were analyzed by fused-disk X-ray fluorescence; S, Ba, Cr, Cu, Li, Ni, Sr, V, Zn, and Zr by 4-acid digestion and inductively coupled plasma-optical emission spectrometry (ICP-OES); Ag, As, Be, Bi, Cd, Co, Ga, Ge, Hf, In, Mo, Nb, Pb, Rb, Sb, Sc, Sn, Ta, Tl, W, and Cs were analyzed by 4-acid digestion and ICP-mass spectrometry (MS); Th, U, Y, and REEs were analyzed by lithium metaborate fusion and ICP-MS; Se and Te by 4-acid digestion, hydride-generation, and atomic absorption spectrometry (AAS), Hg by cold vapor AAS, and Cl^- was analyzed by the specific-ion electrode method. Based on duplicate analyses of 10% of the samples, precision was better than 5% for S, As, Ba, Be, Bi, Cd, Co, Cr, Cu, Ga, Ge, In, Li, Mo, Ni, Pb, Rb, Sc, Se, Sr, Te, Th, Tl, U, V, Zn, REEs, Cl^-, and Cs and better than 10% for Sb, Sn, W, and Hg. For a few elements, precision varies widely and data should be used with that in mind: Ag (10–33%), Hf (11–28%), Nb (15–24%), Ta (13–24%), and Zr (5–16%). Five samples were also analyzed for PGE and Au contents by fire assay and ICP-MS. Analytical accuracy was calculated using international standards AMIS0056 and HGMNEW and is better than 5% for Os and Ru, better than 10% for Ir, Pd, and Pt, 13% for Au, and varies from 5–17% for Rh.

Q-Mode factor analyses used the Varimax method (Klovan and Imbrie 1971). All communalities are >0.94 and values between -0.1575 and 0.1575 were not considered because they are below the level of statistical significance assuming a multi-Gaussian distribution.

The extent of the area covered by seamounts was determined using ArcGIS® and ETOPO bathymetry (Amante and Eakins 2009; http://www.ngdc.noaa.gov/mgg/global/global.html).

Mineralogy and Chemical Composition of Crusts

All Fe-Mn crust samples are composed predominately of δ-MnO_2 (vernadite), the mineral most characteristic of hydrogenetic Fe-Mn deposits found globally. The mineral δ-MnO_2 is epitaxially intergrown with X-ray amorphous iron oxyhydroxide (δ-FeO(OH)-feroxyhyte; Burns and Burns 1977; Varentsov et al. 1991; Hein et al. 2000). Detrital minerals, such as quartz and feldspar, and biogenic and diagenetic minerals, such as calcite and carbonate fluorapatite (CFA) are present in minor to moderate amounts (Table 2). In addition, two samples contain minor amounts of 10 Å manganate (probably todorokite), which may reflect a lower oxidation potential of seawater caused by increased biological productivity, as suggested by Hein et al. (2000) for some occurrences in the Pacific Ocean, or may indicate a minor hydrothermal contribution. Minor amounts of goethite are also present in the majority of the samples and can reflect a number of different processes, including: (1) increased inputs of Fe from continental sources (Bruland et al. 2001); (2) too much Fe present for the vernadite structure to accommodate (De Carlo 1991, and references therein); (3) the enhanced supply of Fe from the dissolution of calcareous tests for crusts below the calcite compensation depth (CCD), as suggested by von Stackelberg et al. (1984) for goethite in some layers of a deep-water Fe-Mn crust (4,830 m) collected in the Clarion-Clipperton nodule belt; and (4) as suggested by Hein et al. (2000), goethite is found only in the older parts of 5% of 640 crust samples analyzed from Pacific Ocean sites and may result from the maturation of X-ray amorphous Fe oxyhydroxide. Most

Table 2. X-ray Diffraction Mineralogy of Fe-Mn samples

Sample	δ-MnO_2 (%)	Others*[2]
3477-B.3.4	95	feldspar; todorokite; quartz; goethite
3478-B.3.5	93	goethite; calcite; plagioclase; quartz
3513-13	94	goethite; plagioclase; quartz
3513-14	94	goethite; quartz; plagioclase
3513-16	85	quartz; goethite; feldspar; kaolinite
3521-6	92	CFA; low Mg-calcite; goethite
3522-4	99	calcite
3708-1	94	quartz; goethite
3709-1	91	quartz; goethite; plagioclase
3710-1	95	quartz; goethite
3711-2	87	calcite; quartz; goethite
3717-12	97	goethite; plagioclase; quartz
3718-1	87	quartz; goethite; aragonite; plagioclase
3525-9	99	calcite; quartz
3533-7	85	CFA; goethite
3534-14.1	93	goethite; feldspar; quartz; calcite
3536-3	71	calcite; Mg-calcite; todorokite; goethite; quartz
3862	96	goethite

*[2]In approximate decreasing abundance; CFA means carbonate fluorapatite.

Atlantic crusts in our study do not originate from below or near the CCD and their Fe concentrations are not greater than those of many crusts without goethite, so that explanations (1) and (4) may be most likely for the occurrence of goethite in the Atlantic samples.

The Fe-Mn crust samples have Fe contents from 12.5 to 23.2 wt% with an average of 17.9 wt% and Mn contents from 9.3 to 17.0 wt% with a mean of 13.7 wt% (Table 3). These concentrations result in Fe/Mn ratios of 0.88 to 1.96 with a mean of 1.33, which is in the range typical of continental margin hydrogenetic Fe-Mn crusts (Hein et al. 2000). Silicon and Al concentrations range from 1.21 to 13.0 wt% and 0.73 to 4.66 wt% with average values of 4.45 and 2.04 wt%, respectively; Si/Al ratios vary between 0.83 and 5.32, with an average value of 2.05. The Si/Al ratios of the volcanic rocks in the area (Geldmacher et al. 2006; Merle et al. 2006) cluster around 2.8. Sample 3708-1 from Unicorn Seamount has a Si/Al ratio of 5.32 indicating the presence of biogenic silica or eolian quartz. An explanation for the low Si/Al ratios is more difficult but preferential incorporation of feldspar over quartz or sorption of Al hydroxide as suggested by Koschinsky and Halbach (1995) could explain those ratios. Calcium concentrations range from 0.99 to 12.7 wt% with a mean value of 3.23 wt%, and P varies from 0.21 to 4.28 wt%, averaging 0.65 wt%.

Cobalt, Cu, and Ni show minimum concentrations of 931, 315, and 1,240 ppm and maximum concentrations of 5,440, 2,050, and 3,980 ppm, respectively. Cobalt has a mean concentration of 3,408 ppm, copper averages 872 ppm, and nickel 2,197 ppm. The Co + Cu + Ni maximum is 0.96 wt%, with a mean of 0.64 wt%. These values and the Fe/Mn ratios are consistent with a predominantly hydrogenetic origin of continental margin Fe-Mn crusts. Some compositional data points fall outside

Table 3. Chemical composition

		3521-6	DUP-3521-6	3522-4	3525-9	3536-3	3708-1	3709-1	3710-1	3711-2	3718-1
Fe	wt%	17.8	N.A.	20.3	22.9	12.5	17.8	16.9	20.8	18.0	17.9
Mn		13.5	N.A.	16.1	14.3	14.2	13.8	15.3	10.6	11.9	12.1
Si		1.21	N.A.	2.20	2.34	3.65	5.94	6.78	4.96	3.87	9.77
Al		1.47	N.A.	1.46	1.33	2.62	3.05	2.07	3.05	1.76	1.84
Ca		6.05	N.A.	2.54	2.16	8.58	1.50	1.72	1.40	5.06	1.49
Mg		1.92	N.A.	1.18	1.09	4.06	1.49	1.21	1.28	1.08	0.98
Na		0.91	N.A.	1.05	1.00	0.53	1.12	1.31	0.87	1.00	1.26
K		0.25	N.A.	0.30	0.29	0.49	0.48	0.51	0.44	0.43	0.60
Ti		1.10	N.A.	0.91	0.98	0.10	0.80	0.61	0.93	0.88	0.50
P		1.46	N.A.	0.42	0.46	0.21	0.41	0.33	0.46	0.38	0.29
S		0.39	0.40	0.32	0.28	0.23	0.26	0.24	0.21	0.25	0.20
Fe/Mn		1.3	–	1.3	1.6	0.9	1.3	1.1	2.0	1.5	1.5
Si/AI		0.83	–	1.51	1.75	1.39	1.95	3.27	1.62	2.20	5.32
Ag	ppm	0.29	0.10	0.34	0.23	0.04	0.12	0.12	0.11	0.11	0.24
As		455	416	317	373	328	250	233	298	272	244
Ba		884	904	1270	1450	953	977	1240	740	882	1540
Be		9.5	9.0	11	12	3.7	9.3	8.6	8.3	7.8	8.7
Bi		33	31	31	25	6.5	22	24	24	22	16
Cd		4.0	3.7	4.6	4.0	2.8	7.4	3.8	5.3	2.9	2.4
Co		5440	5230	4000	3380	931	3250	3440	3180	3260	2510
Cr		101	109	21	78	61	49	121	54	35	30
Cu		426	422	784	592	317	1420	1040	786	368	1410
Ga		8.6	8.1	9.6	13	7.8	14	15	13	9.8	14
Ge		0.8	0.8	0.7	0.9	0.2	0.6	0.5	0.6	0.7	0.4
Hf		8.4	3.7	8.2	3.9	0.36	3.3	1.7	3.3	1.6	7.1
In		0.12	0.11	0.10	0.12	0.05	0.12	0.14	0.20	0.10	0.13

Li	ppm	18	18	8	6	117	49	22	22	11	11
Mo		328	314	444	464	184	308	387	228	299	446
Nb		68	36	58	50	5.2	34	41	41	31	43
Ni		2350	2420	1830	1400	2790	2570	2650	1290	1240	1440
Pb		1860	1930	1880	1740	519	1110	1230	1120	1320	1000
Rb		5.4	4.9	6.1	6.6	18	14	14	15	15	19
Sb		46	39	46	57	26	38	45	43	32	47
Sc		20	18	13	16	12	15	11	20	14	9.1
Se		<0.2	<0.2	0.4	0.5	<0.2	0.5	0.3	0.6	0.4	<0.2
Sn		7.6	6.7	5.4	5.3	1.7	4.8	6.3	10	4.9	4.4
Sr		1380	1400	1290	1320	557	849	1040	719	1070	916
Ta		2.3	1.2	1.8	1.8	O.05	0.85	0.42	1.2	0.60	0.63
Te		71	67	47	42	11	34	43	46	42	32
Th		54	54	37	44	24	40	46	75	66	49
Tl		118	112	142	49	38	116	140	75	65	60
U		15	15	14	14	4.7	11	10	11	12	6.6
V		914	997	962	1030	599	737	660	795	793	764
W		64	50	109	108	36	66	80	48	64	53
Zn		463	475	557	560	566	594	548	473	435	622
Zr		214	240	137	72	16	173	57	180	212	128
La		356	343	294	371	53.8	196	211	229	327	141
Ce		1120	1080	1270	1570	250	1100	1370	1540	1360	1280
Pr		77.8	74.8	66.9	84.1	14.2	49.1	51.7	57.8	80.1	32.3
Nd		297	286	251	316	55.3	186	188	214	298	112
Sm		70.1	66.8	57.2	71.6	15.8	46.6	43.6	53.2	70.0	25.8
Eu		16.7	16.2	13.9	17.1	3.79	11.0	10.1	13.1	16.3	5.68
Gd		77.7	74.1	63.3	78.4	17.6	50.0	42.2	58.5	71.2	22.6
Tb		12.1	11.6	9.99	12.3	2.96	8.27	6.62	9.34	11.0	3.62

(*Continued*)

Table 3. Continued

		3521-6	DUP-3521-6	3522-4	3525-9	3536-3	3708-1	3709-1	3710-1	3711-2	3718-1
Dy		65.0	62.4	50.8	63.2	15.9	43.0	33.2	49.1	55.3	17.1
Y		340	333	184	230	77.9	164	103	182	186	46.1
Ho		14.9	14.3	11.1	13.5	3.50	9.54	7.03	10.7	11.6	3.35
Er		42.1	41.3	29.7	37.6	10.1	26.8	19.2	30.0	31.4	9.45
Tm		5.90	5.81	4.29	5.21	1.48	3.96	2.74	4.50	4.30	1.38
Yb		35.6	34.7	26.1	32.1	8.9	24.6	17.3	28.0	25.6	8.8
Lu		5.62	5.37	3.93	4.73	1.34	3.87	2.60	4.32	3.75	1.37
Hg	ppb	14	14	13	7	7	10	8	25	11	10
Cl^-	ppm	>5000	>5000	>5000	>5000	3120	>5000	>5000	>5000	>5000	>5000

		3862	3477-B.3.4	3478-B.3.5	3513-13	DUP-3513-13	3513-14	3513-16	3533-7	3534-14.1	3717-12
Fe	wt%	23.2	17.6	16.6	16.6	N.A.	15.7	12.6	14.0	21.4	20.3
Mn		13.3	17.0	16.3	13.4	N.A.	13.2	9.3	13.5	13.2	15.5
Si		1.57	3.09	3.36	4.47	N.A.	5.94	13.0	1.30	2.48	2.32
Al		1.29	1.74	1.73	2.45	N.A.	2.65	4.66	0.73	1.49	1.23
Ca		2.04	1.92	3.34	1.40	N.A.	1.28	0.99	12.7	2.17	1.87
Mg		1.24	1.48	1.57	1.32	N.A.	1.36	1.83	1.13	1.32	1.10
Na		1.13	1.25	1.16	1.22	N.A.	1.13	1.27	0.84	0.98	1.14
K		0.24	0.51	0.49	0.45	N.A.	0.68	1.59	0.37	0.31	0.46
Ti		2.37	0.67	0.57	0.83	N.A.	0.52	0.74	0.29	1.01	0.32
P		0.51	0.38	0.41	0.39	N.A.	0.31	0.24	4.28	0.51	0.31
S		0.29	0.30	0.26	0.24	0.23	0.18	0.14	0.31	0.27	0.26
Fe/Mn		1.7	1.0	1.0	1.2	–	1.2	1.4	1.0	1.6	1.3
Si/Al		1.21	1.77	1.95	1.82	–	2.24	2.79	1.79	1.66	1.88
Ag	ppm	0.44	0.34	0.14	0.12	0.15	0.18	0.23	0.05	0.12	0.04

As	ppm	439	316	278	214	213	207	129	279	419	346
Ba		1450	1320	1360	955	958	1170	769	2180	991	1550
Be		12	8.8	8.0	7.2	7.1	8.1	5.5	7.3	12	11
Bi		15	30	23	18	18	18	14	15	24	25
Cd		4.6	3.7	4.0	4.7	4.6	5.0	3.8	2.5	3.4	2.7
Co		4270	4930	4060	3860	3800	2020	1650	2640	4330	1970
Cr		72	51	50	31	33	67	27	49	60	111
Cu		382	970	969	1140	1130	2050	2010	315	454	449
Ga		14	16	16	14	14	19	19	8.0	10	13
Ge		1.0	0.5	0.5	0.7	0.7	0.6	0.3	0.4	0.7	0.6
Hf		6.5	12	5.8	2.4	3.1	5.5	7.3	0.86	3.0	1.2
In		0.10	0.14	0.11	0.19	0.19	0.29	0.31	0.06	0.09	0.16
Li		11	26	33	27	26	43	63	13	11	7
Mo		371	379	341	289	289	360	164	278	350	548
Nb		74	68	41	29	41	43	58	11	50	11
Ni		1330	3670	3980	2010	1990	2590	2590	1990	1590	2210
Pb		991	2100	1720	943	953	863	539	1330	1650	1060
Rb		3.2	12	12	12	12	20	34	8.3	6.5	11
Sb		47	55	48	32	32	34	27	37	47	56
Sc		21	10	8.6	14	14	13	17	7.4	17	11
Se		0.3	<0.2	<0.2	0.3	0.3	<0.2	0.3	<0.2	0.4	<0.2
Sn		8.1	7.2	5.5	3.8	3.8	3.7	3.4	2.1	5.0	4.9
Sr		1340	1130	1030	1090	1060	745	484	1470	1090	1170
Ta		4.1	1.2	0.60	0.84	1.1	0.99	1.8	0.38	1.2	0.12
Te		49	66	56	40	41	25	33	32	58	34
Th		43	39	37	61	59	69	50	17	52	45
Tl		73	195	169	122	123	120	61	85	73	143
U		19	9.7	8.6	9.6	9.3	7.6	5.1	9.2	14	8.3

(*Continued*)

Table 3. Continued

		3862	3477-B.3.4	3478-B.3.5	3513-13	DUP-3513-13	3513-14	3513-16	3533-7	3534-14.1	3717-12
V		1130	848	797	662	644	612	270	861	974	904
W		54	115	92	57	57	64	25	84	72	121
Zn		650	724	755	468	475	604	547	576	538	652
Zr		75	151	88	122	178	204	104	88	139	55
La		390	190	174	282	270	189	120	181	324	265
Ce		1460	1210	1100	1450	1400	1290	972	662	1260	1400
Pr		90.8	40.8	39.2	70.3	67.2	52.8	30.9	36.8	71.7	61.8
Nd		339	153	145	254	244	191	113	142	269	229
Sm		78.9	34.4	33.4	61.6	59.2	48.3	27.9	31.9	62.7	52.4
Eu		18.8	8.10	7.85	14.5	13.8	11.2	6.50	7.38	14.9	12.4
Gd		85.0	35.0	34.4	62.0	59.5	46.6	27.0	36.1	68.5	51.1
Tb		13.6	5.61	5.30	9.87	9.55	7.37	4.32	5.62	10.8	7.87
Dy		69.8	29.0	26.8	49.3	47.5	36.5	21.6	30.7	55.8	38.4
Y		269	110	100	164	158	120	79.9	159	217	111
Ho		15.4	6.29	5.85	10.4	9.92	7.49	4.52	7.12	12.4	8.03
Er		41.8	17.6	16.1	27.9	27.1	20.8	11.9	20.0	34.0	21.4
Tm		5.82	2.48	2.26	4.03	3.80	2.92	1.78	2.84	4.80	2.97
Yb		35.0	15.5	14.0	23.8	23.6	18.4	11.1	17.3	29.3	18.3
Lu		5.19	2.48	2.26	3.76	3.54	2.75	1.68	2.67	4.42	2.81
Hg	ppb	292	7	8	8	9	6	8	6	9	8
Cl^-	ppm	>5000	>5000	>5000	>5000	>5000	>5000	>5000	3640	>5000	>5000

All Cs concentrations <5 ppm.

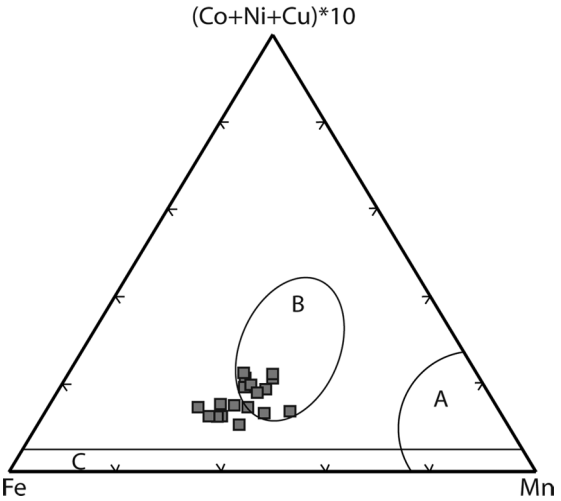

Figure 2. Ternary diagram. All data plotted as wt %. The fields are: (A) diagenetic, (B) hydrogenetic, and (C) hydrothermal. Ternary plot software from (www.crog.org/cedric/dplot).

the typical open-ocean hydrogenetic field (Figure 2), but do fall within the field typical for Pacific continental margin and small ocean basin Fe-Mn crusts. These continental-margin-type crusts show lower total Co + Cu + Ni and higher Fe, Si, Al, and Cr contents than open-ocean crusts, reflecting the higher terrigenous input per unit area for the Atlantic (Koschinsky et al. 1995; Hein et al. 2000).

Tellurium is also an important element because of its potential economic value in the solar cell industry (Hein et al. 2010). In our samples, Te ranges from 11 to 71 ppm with an average value of 43 ppm. Hein et al. (2003) reported mean concentrations of Te for Pacific and Atlantic hydrogenetic Fe-Mn crusts of 50 ppm, which is consistent with our data. Vanadium, W, Zr, and Th also have notably high concentrations in our samples (Table 3).

Differences in crust composition based on subregions of our study area (Mediterranean, Canaries, Tore, Maderia-Tore Rise (MTR), and Azores) are presented in Figure 3 using data averaged from Table 3 for each subregion (see Table 1). It should be stressed that for Mediterranean and Azores subregions, only one sample is available, which should be taken in to consideration when comparing to the average values from the remaining subregions. We also distinguish between the different MTR seamounts: MTR-Josephine and South MTR seamounts (which includes Nameless, Unicorn, Seine and Godzilla seamounts). South MTR seamounts is the subregion with the highest average values of Co + Ni + Cu, Co, Ni, Zn, Mo, Tl, W, Te, and Bi. The Mediterranean subregion is systematically lower for all elements, with the exceptions of Ni and Zn. The Canaries subregion shows the highest P contents, which will be discussed in the section on phosphatization, and the Azores subregion shows the higher concentrations of Ti (2.37 wt%), which may include a significant detrital source as well as the typical adsorption of Ti from seawater.

Changes in the geochemical composition of Fe-Mn crusts with water depth, such as increased Cu, Ni, Si, and Al concentrations with increasing water depth have been identified previously (e.g., Cronan 1977, 1997; Mangini et al. 1987; Hein et al. 1997). Increased Ni contents with water depth are not found in our sample set (Figure 4).

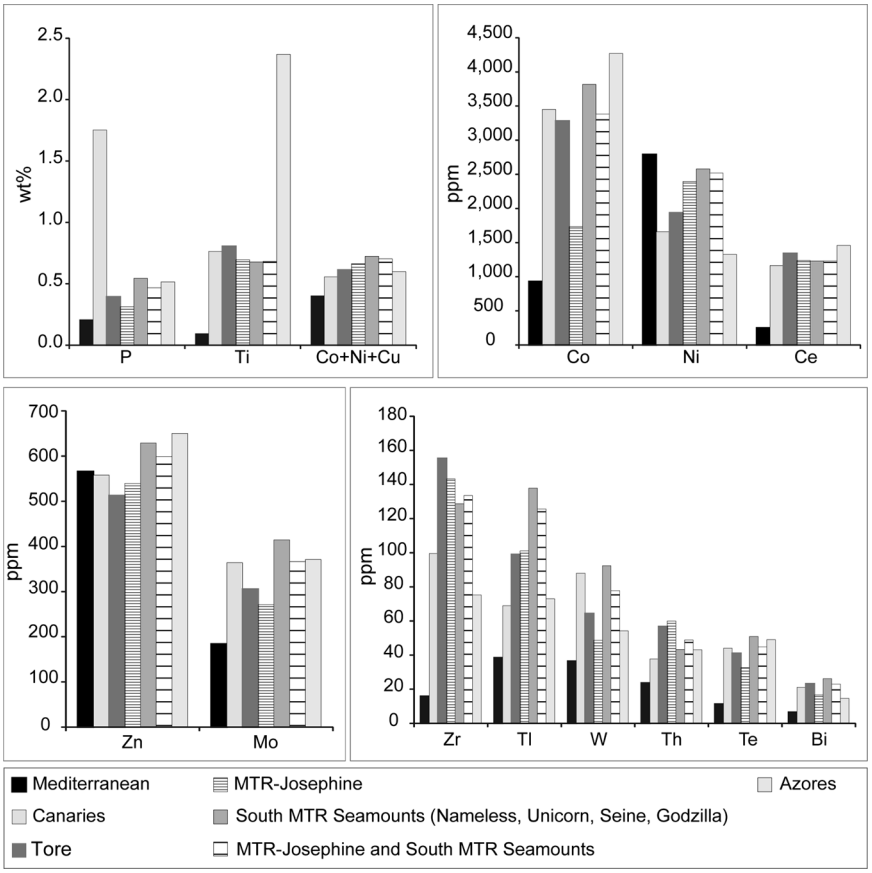

Figure 3. Trace-metal concentrations in different subregions of the study area. Data correspond to averages of analyses in Table 3 (See also Table 1).

There is an apparent increase of Cu content with water depth, which might be caused by the release of Cu during dissolution of carbonate material close to the CCD (Halbach et al. 1979 and references therein; Cronan 1997; Verlaan et al. 2004). Planktonic organisms extract metals from surface waters for metabolic processes and through scavenging. Dissolution of the carbonate tests and oxidation of the organic matter then release these metals at depth. The CCD in the North Atlantic lies at about 4,700–4,800 m (van Andel 1975; Broecker and Peng 1982). Our most Cu-enriched samples are from ~4,600 m water depth. Cronan (1997) found that for Pacific manganese nodules, the highest Cu contents are not present in the deepest water nodules below the CCD, but in those located slightly above the CCD at around 5,000 m water depth. The increased deep-water Cu concentrations may thus be the result of a reduction in sedimentation rate associated with the loss of carbonate tests by dissolution near the CCD. That loss would lead to an increase in the concentration of organic phases in the sediments, whose decay would promote diagenetic reactions that enrich Cu and increase Al and Si contents (Cronan 1997). Our dataset supports this and shows similar increases with water depth for Cu, Al, and Si, and an opposite trend for Ca (Figure 4). Dissolution of carbonate tests may influence geochemistry

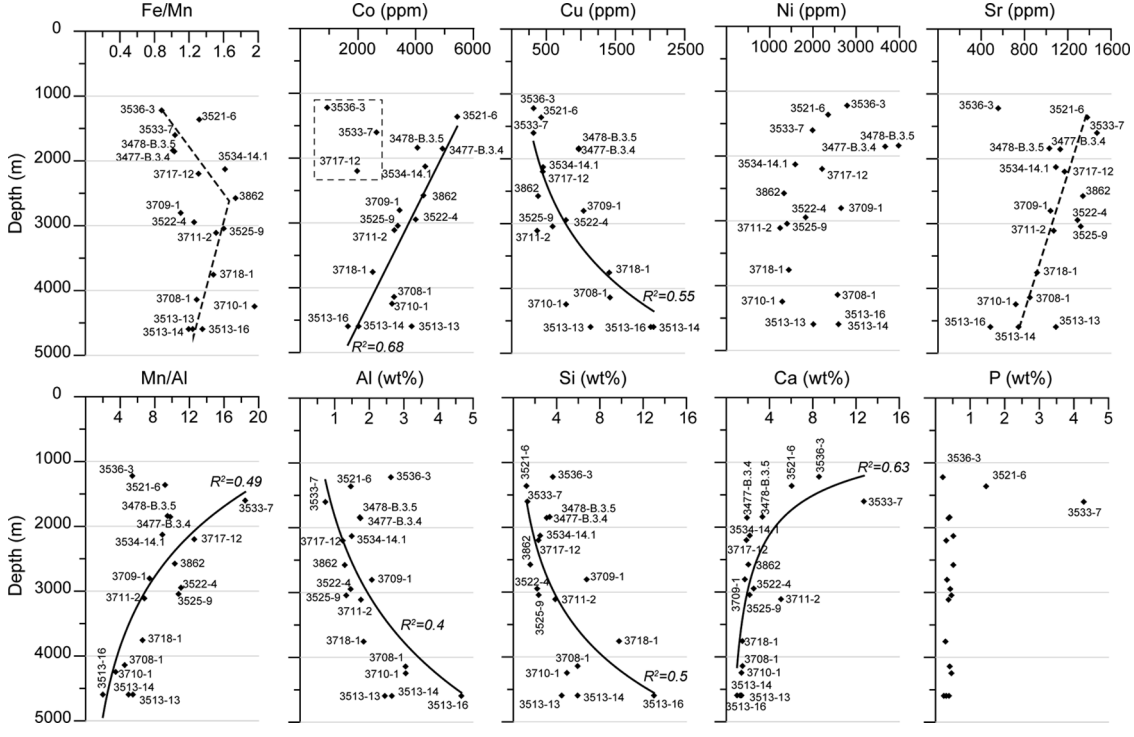

Figure 4. Distribution of selected elements with water depth. Dashed lines correspond to hand-drawn trends, others are regression lines; dashed box in Co illustrates the group of samples not considered for regression lines.

within the calcite lysocline at depths from about 2,600 to 3,000 m as indicated by a significant change in the slope of the Ca pattern and a change from increasing Fe/Mn to decreasing Fe/Mn with depth (Figure 4).

Rare Earth Elements

Chondrite-normalized REE patterns (Figure 5a) show enrichment of lightREEs (LREEs) relative to heavyREEs (HREEs), a strong positive Ce anomaly, and a small positive Gd anomaly, which are typical of Fe-Mn crusts of hydrogenetic origin. Shale-normalized patterns (Figure 5b) are also characteristic of hydrogenetic Fe-Mn crusts in that they show pronounced middleREEs (MREEs) enrichment (Nath et al. 1992 and references therein). No direct relationship with water depth or geographic location is discernable, with the exception of crust 3536-3 from the Mediterranean Sea in which REEs concentrations are much lower. All samples are highly enriched in REEs relative to seawater and the Earth's crust, with up to 0.29 wt.% total REEs, crust 3536-3 being the exception with only 475 ppm total REEs. This sample grew in the Mediterranean Sea and precipitation of the oxides was governed by waters in the Alboran Basin mixed with Atlantic waters that entered through the Strait of Gibraltar. The waters from the Mediterranean are characterized by low oxygen contents and a low redox potential. Also, this sample and sample 3533-7 show less pronounced Ce anomalies. The presence of positive Ce anomalies is caused by scavenging of Ce from seawater by hydrous Fe-Mn oxides (Goldberg et al. 1963; Elderfield et al. 1981) and its preferential retention relative to the other REEs in the oxide phase through surface oxidation (Bau et al. 1996). According to Kuhn et al. (1998), and given that Ce (III) oxidation is characterized by slow reaction kinetics (Sholkovitz and Schneider 1991; Moffet 1994), the size of the Ce anomaly will depend on the duration that the Fe-Mn precipitates are in contact with seawater. De Carlo (1991) suggested that variations in the REEs abundances and the extent of fractionation between LREEs and HREEs primarily reflect changes in the mineralogical composition of the crusts. De Carlo (1991) also pointed out that care must be taken when

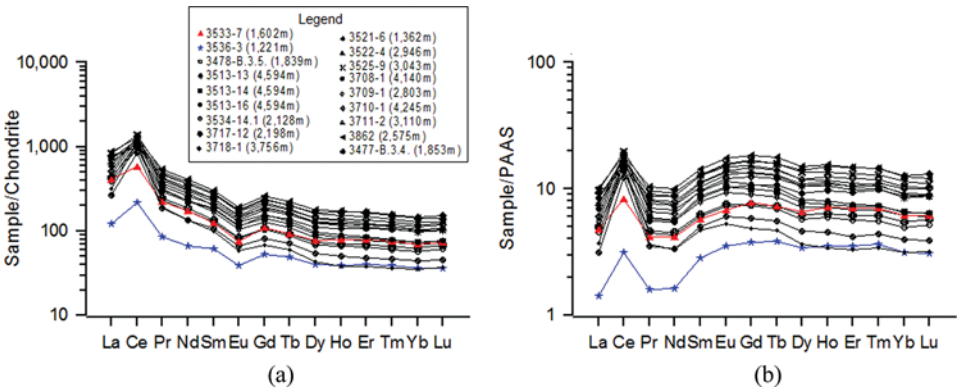

Figure 5. (a) Chondrite-normalized REE patterns. Normalization values from Anders and Grevesse (1989); (b) Shale-normalized REE patterns. Normalization values for Post-Archean Australian Shale from Taylor and McLennan (1985); water depth listed after sample number in the Legend. (Color figure available online.)

using Ce anomalies calculated from bulk REE data as indicators of paleoredox conditions, given that the Ce anomaly is not only sensitive to variations in Ce content but also to variations in the concentrations of trivalent REEs, which are associated primarily with Fe and/or phosphate phases, whereas Ce is associated with the Mn phase. The Ce anomaly may not solely reflect Ce redox cycling and the REEs may provide indirect rather than direct evidence of changes in the depositional conditions that result from controls on the Fe/Mn ratio. Accordingly, the low REE contents of crust 3536-3 are most likely the result of hydrothermal or diagenetic contributions characterized by fast growth rates and high Ni and Li contents.

Platinum-Group Elements

Fe-Mn crusts are highly enriched in PGEs (Ir, Ru, Rh, Pt, Pd), especially Pt, compared to Earth's crustal abundances (Hein et al. 2000). Based on the five samples analyzed for PGEs, the Pt contents vary between 153 and 512 ppb, with an average value of 283 ppb; Rh, Ru, Pd, and Ir show concentrations up to 39, 21, 19, and 10 ppb, respectively (Table 4).

The processes of Pt enrichment in Fe-Mn crusts are not fully understood. Several mechanisms have been proposed for this enrichment, such as reduction or oxidation reactions, diagenetic or cosmogenic input, and enrichment related to phosphatization (Halbach et al. 1989a, 1990; Vonderhaar et al. 2000; Hein et al. 2005). We consider that the oxidative enrichment is the most likely general mechanism for high Pt concentrations; tetravalent Pt would be the final product, as is also the case for Ce, whereas Te is hexavalent (Hein et al. 2003). The most likely mechanism is that Pt is sorbed from seawater and then oxidized on the surface of the FeO(OH) (Hodge et al. 1985; Hein et al. 1997; Hein et al. 2003; Banakar et al. 2007).

Interelement Relationships and Mineral Phases

A correlation coefficient matrix for selected elements (Table 5) shows that Fe is positively correlated (99% Confidence Interval-CI) with Ti, Mo, and REEs (the correlation is better with LREEs and MREEs) and to a lesser extent (95% CI) with Y and Co. Manganese is positively correlated with W, Tl, and Pb at the 99% CI, and also with Zn, Mo, Ni, and Bi at 95% CI, and shows negative correlations with the REEs (except La, Pr, and Nd). Cobalt shows strong positive correlations (99% CI) with Te, Pb, Nb, Bi, and some REEs (La, Pr, Nd, Tb, Dy, Ho, Er, Yb), and the correlations are better with the MREEs and HREEs. Tellurium also shows positive correlations with the same elements as Co, but Te shows lower correlation coefficients with Bi and the REEs. Both Co and Te show higher coefficients with Fe than with Mn and both show negative correlations with elements characteristic of the detrital-aluminosilicate fraction, which was also found for Te in open-ocean crusts (Hein et al. 2003).

Q-Mode factor analysis produces five factors that explain 97.3% of total variance of the data. Considering the mineralogical composition of the samples, we conclude that the five factors represent the Fe oxyhydroxide, aluminosilicate, biogenic (which may also include hydrothermal Mn), hydrogenetic Mn, and CFA phases (Figure 6), which is in agreement with previous work (Muiños 2005) that used a slightly different dataset and statistical tool (Pereira et al. 2003**)** and with investigations of globally distributed crusts (Frank et al. 1999). It is also worth

Table 4. PGE concentrations and ratios in five Fe-Mn crusts

Sample ID	Depth (m)	Fe (wt%)	Mn (wt%)	Co (wt%)	Ce (wt%)	Fe/ Mn	Ir (ppb)	Ru (ppb)	Rh (ppb)	Pt (ppb)	Pd (ppb)	Au (ppb)	Pt/ Pd	Ru/ Rh	Pd/ Ir	Pt/ Ir	Pd/ Ru	Pt/ Ru	Pt/ Au
3533-7	1602	14.0	13.5	0.26	0.07	1.04	5	14	14	153	19	—	8.1	1.0	3.8	31	1.4	11	—
3478-B.3.5	1839	16.6	16.3	0.41	0.11	1.01	10	21	39	512	14	9	37	0.54	1.4	51	0.67	24	57
3534-14.1	2128	21.4	13.2	0.20	0.13	1.62	6	17	25	231	11	—	21	0.68	1.8	39	0.65	14	—
3513-14	4594	15.7	13.2	0.17	0.10	1.20	6	18	18	223	10	—	22	1.0	1.7	37	0.56	12	—
3513-16	4594	12.6	9.3	0.43	0.13	1.35	6	13	27	296	15	—	20	0.48	2.5	49	1.2	23	—

Table 5. Correlation Coefficient Matrix for selected elements

	Fe	Mn	Fe/Mn	Si	Al	Ca	Ti	P	Bi	Co	Cu	Mo	Nb	Ni	Pb	Te	Th	Tl	W	Zn	Zr
Fe																					
Mn	0.167																				
Fe/Mn	0.720	−0.552																			
Si	−0.449	−0.567	0.023																		
Al	−0.473	−0.584	0.036	0.795																	
Ca	−0.434	0.058	−0.417	−0.426	−0.381																
Ti	0.648	−0.153	0.634	−0.234	−0.139	−0.316															
P	−0.241	−0.023	−0.202	−0.358	−0.424	0.794	−0.145														
Bi	0.363	0.489	−0.030	−0.409	−0.459	−0.065	−0.064	0.108													
Co	0.503	0.362	0.187	−0.483	−0.434	−0.153	0.561	0.053	0.597												
Cu	−0.382	−0.291	−0.118	0.802	0.708	−0.549	−0.190	−0.339	−0.138	−0.283											
Mo	0.616	0.564	0.089	−0.313	−0.642	−0.323	0.075	−0.143	0.521	0.246	−0.148										
Nb	0.369	0.004	0.317	0.036	0.047	−0.442	0.664	−0.258	0.318	0.660	0.168	0.088									
Ni	−0.540	0.519	−0.779	0.085	0.191	0.030	−0.423	−0.083	0.040	0.034	0.306	−0.131	0.019								
Pb	0.442	0.587	−0.017	−0.567	−0.599	0.029	0.153	0.164	0.851	0.798	−0.356	0.441	0.462	0.145							
Te	0.463	0.301	0.224	−0.402	−0.343	−0.181	0.469	0.000	0.547	0.928	−0.280	0.185	0.692	0.122	0.809						
Th	0.198	−0.458	0.512	0.320	0.337	−0.564	0.203	−0.418	0.084	0.135	0.395	−0.042	0.225	−0.302	−0.084	0.147					
Tl	−0.018	0.722	−0.481	−0.205	−0.183	−0.233	−0.141	−0.088	0.486	0.465	0.165	0.369	0.194	0.683	0.519	0.468	0.003				
W	0.411	0.821	−0.224	−0.546	−0.622	−0.057	−0.152	0.064	0.706	0.345	−0.294	0.738	0.004	0.223	0.707	0.342	−0.280	0.626			
Zn	−0.005	0.572	−0.383	−0.051	−0.207	−0.116	−0.095	−0.078	−0.048	−0.004	0.140	0.363	0.065	0.605	0.166	0.081	−0.471	0.477	0.427		
Zr	0.109	−0.289	0.315	0.027	0.122	−0.173	0.186	−0.014	0.399	0.406	0.242	−0.106	0.346	−0.166	0.289	0.357	0.679	0.146	−0.146	−0.395	
La	0.797	0.074	0.577	−0.561	−0.510	−0.184	0.721	0.002	0.404	0.642	−0.453	0.432	0.413	−0.542	0.471	0.525	0.276	−0.012	0.284	−0.315	0.275
Ce	0.757	−0.019	0.655	−0.029	−0.142	−0.722	0.506	−0.377	0.367	0.438	0.106	0.545	0.390	−0.412	0.282	0.400	0.652	0.183	0.285	−0.122	0.317
Pr	0.771	0.011	0.605	−0.508	−0.418	−0.232	0.733	−0.034	0.362	0.614	−0.375	0.368	0.392	−0.559	0.403	0.486	0.383	−0.001	0.220	−0.377	0.347
Nd	0.782	0.037	0.590	−0.527	−0.433	−0.225	0.728	−0.069	0.347	0.587	−0.405	0.385	0.382	−0.549	0.395	0.456	0.341	−0.037	0.230	−0.356	0.296
Sm	0.734	−0.079	0.624	−0.443	−0.318	−0.248	0.751	−0.119	0.265	0.504	−0.319	0.304	0.374	−0.609	0.263	0.347	0.394	−0.129	0.087	−0.435	0.363
Eu	0.569	−0.128	0.529	−0.285	−0.356	−0.110	0.684	0.078	0.328	0.542	−0.249	0.292	0.491	−0.441	0.388	0.449	0.314	−0.093	0.094	−0.244	0.365
Gd	0.739	−0.050	0.621	−0.554	−0.363	−0.143	0.770	0.013	0.301	0.576	−0.417	0.230	0.421	−0.558	0.357	0.452	0.299	−0.119	0.131	−0.402	0.338
Tb	0.530	0.433	0.153	−0.665	−0.501	−0.067	0.324	0.198	0.520	0.622	−0.305	0.371	0.116	−0.045	0.590	0.510	0.211	0.499	0.576	−0.030	0.319
Dy	0.724	−0.040	0.607	−0.589	−0.392	−0.110	0.737	−0.010	0.315	0.611	−0.462	0.213	0.394	−0.545	0.384	0.492	0.330	−0.110	0.098	−0.430	0.399
Y	0.559	−0.053	0.476	−0.614	−0.390	0.124	0.693	0.234	0.338	0.649	−0.505	0.065	0.440	−0.435	0.433	0.531	0.113	−0.134	0.033	−0.427	0.371
Ho	0.639	0.328	0.307	−0.653	−0.508	−0.103	0.676	0.142	0.217	0.611	−0.362	0.337	0.273	−0.173	0.402	0.478	0.114	0.317	0.371	0.085	0.166
Er	0.729	0.076	0.536	−0.607	−0.387	−0.109	0.728	0.051	0.420	0.682	−0.427	0.221	0.408	−0.444	0.474	0.524	0.205	−0.013	0.210	−0.347	0.341
Tm	0.493	0.002	0.366	−0.394	−0.335	0.027	0.669	0.076	0.200	0.423	−0.348	0.205	0.504	−0.292	0.254	0.325	−0.105	−0.227	0.018	−0.095	−0.022
Yb	0.706	−0.018	0.590	−0.599	−0.426	−0.021	0.743	0.114	0.358	0.627	−0.505	0.210	0.471	−0.548	0.434	0.526	0.239	−0.083	0.127	−0.415	0.395
Lu	0.293	−0.056	0.259	−0.349	−0.258	0.096	0.720	0.128	−0.032	0.486	−0.316	0.027	0.521	−0.163	0.118	0.403	−0.042	−0.058	−0.221	−0.082	0.142
H2O Depth	−0.002	−0.561	0.385	0.661	0.651	−0.626	0.093	−0.371	−0.167	−0.259	0.748	−0.146	0.050	−0.282	−0.455	−0.323	0.658	−0.162	−0.371	−0.299	0.342

Correlation Coefficient matrix 18 samples
n= 18 for all elements
95% confidence level is |0.468|
99% confidence level is |0.582|

Table 5. Continued

	Zr	La	Ce	Pr	Nd	Sm	Eu	Gd	Tb	Dy	Y	Ho	Er	Tm	Yb	Lu
La	0.275															
Ce	0.317	0.672														
Pr	0.347	0.985	0.711													
Nd	0.296	0.989	0.684	0.993												
Sm	0.363	0.950	0.646	0.972	0.978											
Eu	0.365	0.834	0.584	0.816	0.822	0.793										
Gd	0.338	0.957	0.582	0.961	0.969	0.964	0.790									
Tb	0.319	0.662	0.527	0.690	0.667	0.575	0.447	0.641								
Dy	0.399	0.947	0.547	0.953	0.959	0.960	0.763	0.981	0.626							
Y	0.371	0.848	0.305	0.829	0.835	0.833	0.736	0.911	0.545	0.926						
Ho	0.166	0.740	0.528	0.762	0.747	0.686	0.566	0.749	0.868	0.713	0.633					
Er	0.341	0.913	0.545	0.917	0.921	0.906	0.754	0.950	0.701	0.946	0.919	0.760				
Tm	−0.022	0.662	0.257	0.595	0.641	0.633	0.745	0.690	0.200	0.657	0.759	0.434	0.701			
Yb	0.395	0.895	0.483	0.892	0.889	0.882	0.736	0.944	0.614	0.939	0.929	0.723	0.904	0.667		
Lu	0.142	0.530	0.098	0.499	0.507	0.534	0.589	0.575	0.158	0.592	0.723	0.472	0.554	0.791	0.654	
H2O Depth	0.342	−0.064	0.454	0.059	0.013	0.128	0.010	0.001	−0.106	−0.051	−0.218	−0.123	−0.038	−0.236	−0.141	−0.298
	Zr	La	Ce	Pr	Nd	Sm	Eu	Gd	Tb	Dy	Y	Ho	Er	Tm	Yb	Lu

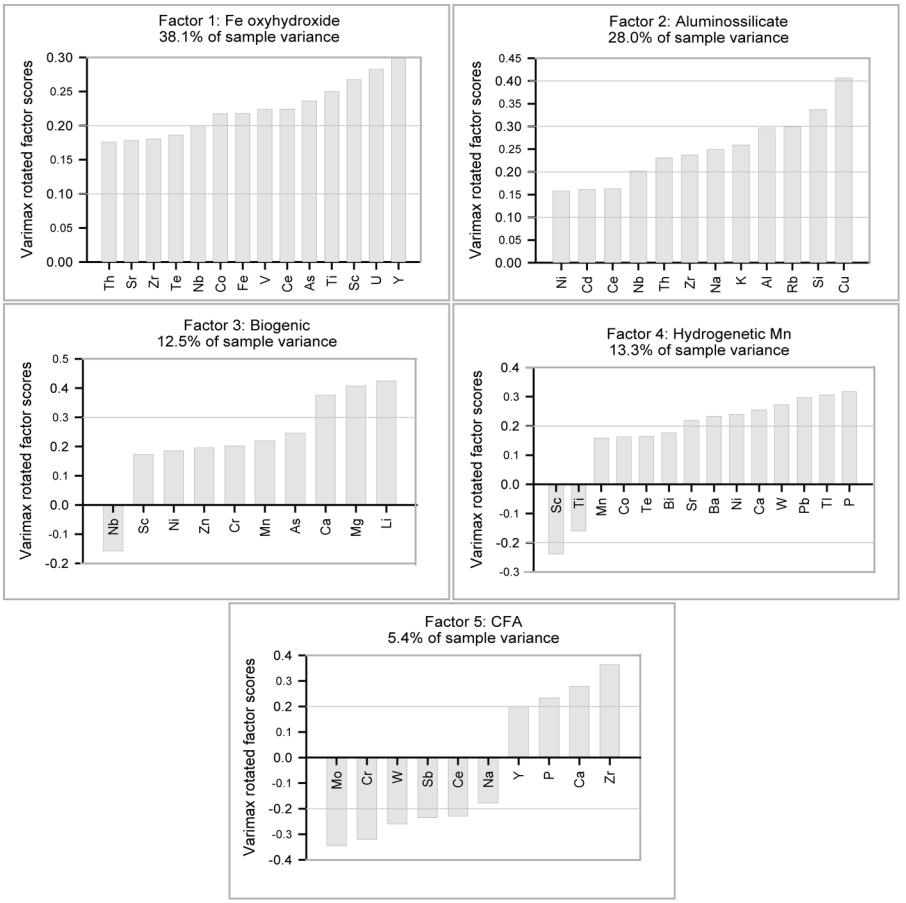

Figure 6. Graphic display of Q-Mode rotated factor scores for five factors; CFA means carbonate fluorapatite.

noting that the fact that the number of samples is smaller than the number of variables does not affect the results, as discussed in Muiños (2005). The identified phases are comparable to the phases commonly found for Pacific and Indian Ocean Fe-Mn crusts.

Phosphatization

Phosphorus contents of our data set vary from 0.21 to 0.51 wt% (a factor of two) throughout the entire region and water depths (Figure 4). However, two samples, 3521-6 (Seine seamount) and 3533-7 (Annika seamount) are exceptions in that they show high P contents of 1.46 and 4.28 wt%, respectively, consistent with the CFA mineral component (Table 2). Regardless of these two samples, P seems to increase to the North and South of the Gibraltar: Samples from the MTR area (MTR-Josephine, Nameless, Unicorn, and Godzilla seamounts) show average P contents of 0.34 wt% while samples to the North (Tore) and South (Canaries) show higher average P values of 0.40 and 0.49 wt%, respectively.

Based on our limited dataset, phosphatization took place within the water-depth range of 1,200 to 1,500 m, but may also have occurred at shallower depths. That water-depth range corresponds to the lower core of MOW characterized by low dissolved oxygen contents and therefore low oxidation potential. This relationship was also pointed out by Koschinsky et al. (1996) and provides an indication of the influence of the prevailing oceanographic conditions in the area on the compositions of the crusts. Hein et al. (1993) suggested that during stable, warm climatic conditions dissolved phosphorous derived from intense chemical weathering on continents accumulated in the deep sea in large quantities. With the expansion of Antarctic glaciation and intensification of ocean circulation, the phosphorous-rich deep waters were redistributed by upwelling and turbulent mixing at the seamounts to intermediate water depths and may have been temporarily stored in the OMZ. Koschinsky and Halbach (1995) proposed a model for precipitation of hydrogenetic Fe-Mn crusts, with crusts being formed below the OMZ, as the result of the mixture of Mn^{2+}-rich and O_2-poor waters with Mn^{2+}-poor and O_2-rich deep waters. Halbach et al. (1982, 1989b) and Koschinsky et al. (1997) linked the phosphatization with the expansion of the OMZ as the result of increased surface-water productivity. The expansion of the OMZ led to the impregnation with CFA of the extant crusts. Despite the fact that a phosphatized old crust generation is missing in Atlantic crusts, Koschinsky et al. (1996) noted phosphatization episodes within a 8.5 Ma record from a crust collected from Lion Seamount in the NE Atlantic Ocean, which may at least in part correspond to the 6 Ma event of phosphatization of limestone that occurred on Lighthill seamount off Morocco (Jones et al. 2002). The phosphatization was most likely a consequence of episodes of increased productivity and biogenic particle flux and is much younger than the phosphatization episodes in the Pacific (Hein et al. 1993).

Thus, the most probable explanation for shallow-water phosphatization is an interaction of the OMZ and MOW to produce an extended depth range for O_2-poor and Mn^{2+}-and dissolved P-rich waters, which reached down the slopes of some seamounts covered with Fe-Mn crusts. As a consequence, crust accretion may have been prohibited and precipitation of CFA promoted at these relatively shallow depths in the Atlantic Ocean (Hein et al. 2000 and references therein).

Resource Considerations

Fe-Mn deposits in the Portuguese EEZ may become an important future resource but there is a clear need for studies to better understand their origin and distribution. During the oceanographic cruises mentioned above, as well as during the SO 83 cruise (Halbach and Scientific Crew 1993), samples of Fe-Mn nodules and crusts were collected on various seamounts from the northeast Atlantic. Despite the fact that the sampling was not systematic, and knowledge of the area needs to be augmented, we present a first-order evaluation of the possible resource potential of Fe-Mn crusts within and adjacent to the Portuguese EEZ, based on criteria developed by Hein et al. (2009).

Grade

According to Hein et al. (2009), large seamount summit areas with high grades of Co, Ti, REEs, Te, Ni, Th, Mn, Pt, etc, will be preferentially chosen for mining the crusts. It is also stressed that the grade will depend on the ability to collect Fe-Mn crusts without their substrate rocks, which would of course result in a decrease in the metal

grade. Figure 7 shows the concentrations of selected trace metals that offer an economic potential for the future, for the crusts analyzed here compared to data for crusts from different ocean basins (from Hein 2004). Average metal concentrations in our dataset are comparable to average concentrations for Indian Ocean Fe-Mn crusts except for Zr, which is significantly higher in Indian Ocean crusts. For most of the metals, average concentrations for our dataset are in the range of the average Atlantic concentrations given by Hein (2004), except also for Zr and

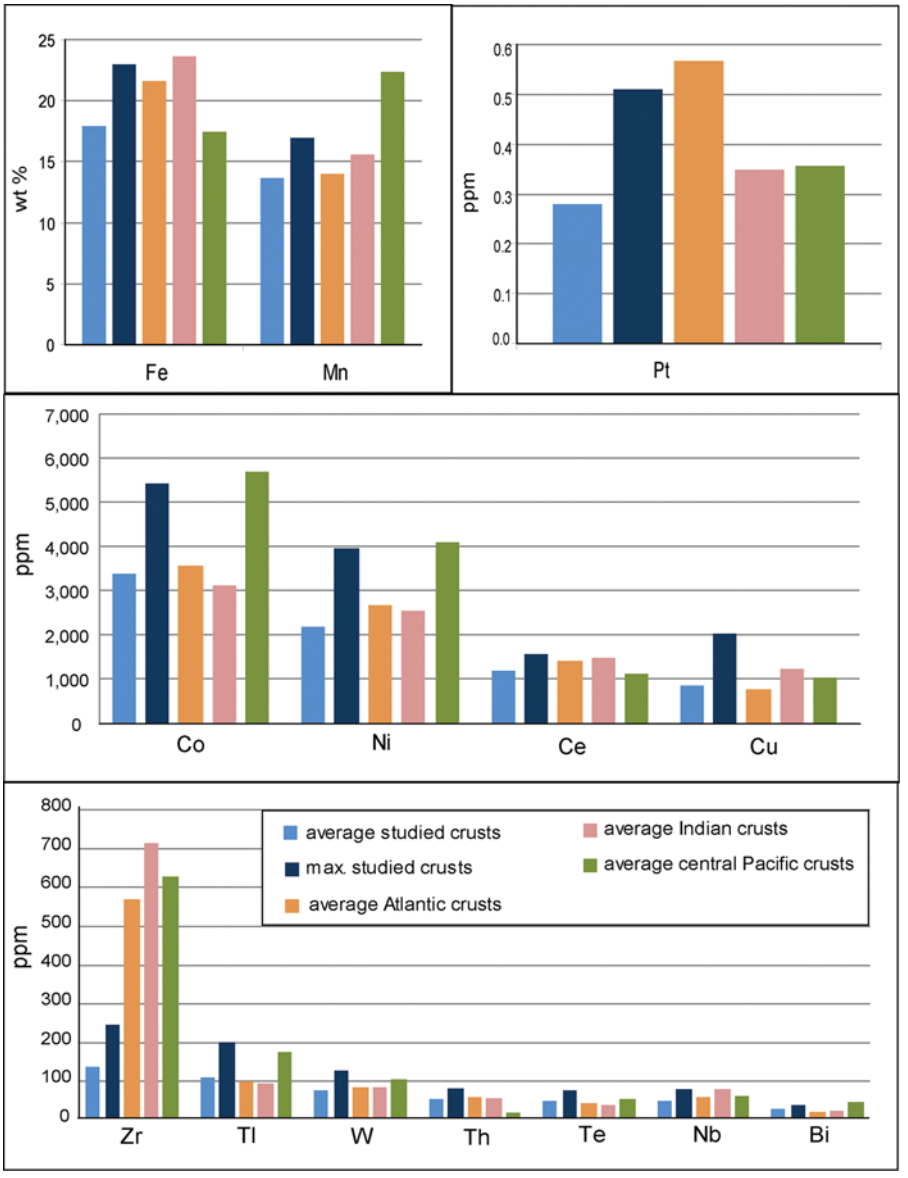

Figure 7. Trace-metal concentrations in different ocean basins and in crusts analyzed here. Mean concentrations for Atlantic, Indian, and central Pacific crusts from Hein (2004). (Color figure available online.)

Pt. In comparison to central Pacific crusts, the average compositions of the crusts analyzed here are systematically lower, with the exceptions of Th, which is enriched in Atlantic and Indian crusts, and Te and Ce, which show similar concentrations. Nevertheless, if we consider the maximum values for our samples, the concentrations are similar to average central Pacific concentrations, except once again for Zr. The highest Co concentrations in our crusts of up to 0.54% Co are found in the shallower-water samples (on Seine and Nameless Seamounts; Figure 4). Further exploration is warranted within those areas and also regionally to possibly locate larger areas with mean crust grades similar to the maximum concentrations found for individual crusts analyzed here.

Tonnage (Thickness)

Tonnages were calculated based on average thicknesses of crusts in our dataset for Nameless, Unicorn, and MTR seamounts (Table 6). Considering data in Table 6, the surface area above 2,500 m water depth, and a mean wet-bulk density of crusts of 1.95 g/cm^3, we calculate the crust tonnage for Nameless, Unicorn, and MTR to be 7.1×10^7, 1.3×10^8, and 1.1×10^9 metric tons of wet crust respectively.

Considering the average concentrations for Co, Ni, Ce, Te, and Pt of 0.34%, 0.22%, 0.13%, 0.0043% and 3×10^{-8}%, respectively, we calculate maximum tonnages of these metals (Figure 8 and Table 6) with consideration for dilution resulting from recovery of substrate rock and unavailability of crusts for recovery due to other factors (see Hein et al. 2009 for discussion).

Area Permissible for Crust Coverage

Due to the absence of detailed sampling and the lack of backscatter side-scan sonar data, a comprehensive and more accurate calculation of the area of crust-coverage is not possible. Despite these limitations, we calculated surface areas using ArcMap's 3D analyst, ArcGIS® from ETOPO bathymetry and present those data considering reductions in areas potentially exploitable that result from water depth constraints, limitations in our knowledge of sediment cover and topography, and the necessity for biological corridors, based on the case study of Hein et al. (2009). The 2,500 m water depth limit proposed by Hein et al. (2009) is also used here even though some Fe-hosted metals increase with water depth, especially copper, which shows increased concentrations in crusts deeper than 3,000 m (Figure 4). We consider that the 2,500 m

Table 6. Calculation of seamount and ridge surface areas for selected seamounts in the study area, crust mean thicknesses, and metric tons of selected metals based on a crust mean wet-bulk density of 1.95 g/cm^3

Seamount	Mean Thickness (cm)	Surface area above 2,500 m water depth (km^2)	Co (Tons)	Ni (Tons)	Ce (Tons)	Te (Tons)	Pt (Tons)
Nameless	8	454	2.4×10^5	1.6×10^5	9.0×10^6	3.0×10^3	2.1×10^{-2}
Unicorn	4	1948	4.5×10^5	2.9×10^7	1.7×10^5	5.7×10^3	4.0×10^{-2}
MTR	7	8492	3.8×10^6	2.5×10^8	1.4×10^6	4.8×10^4	3.4×10^{-1}

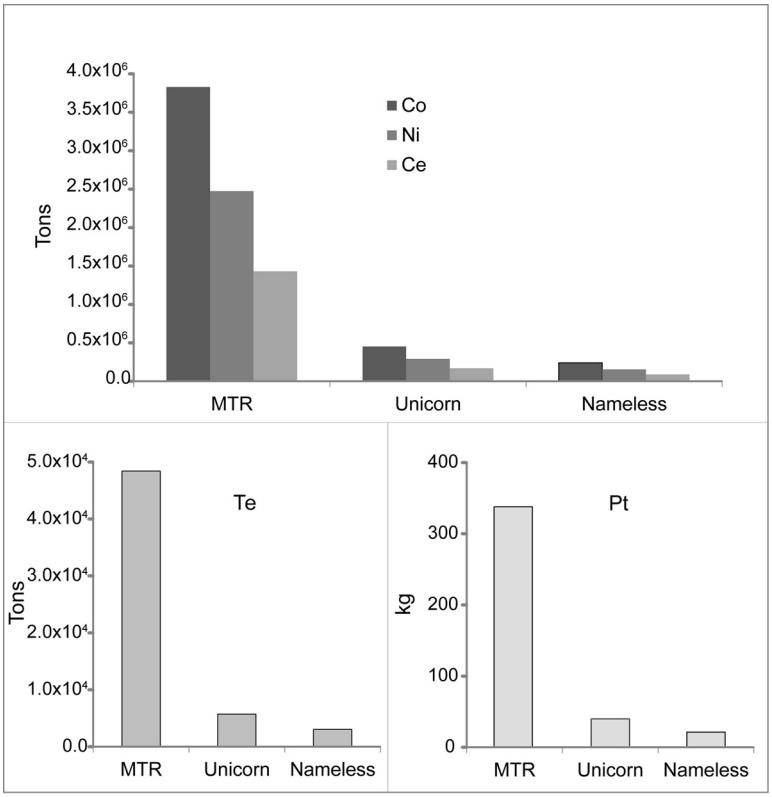

Figure 8. Histogram of metric tons for different metals on the basis of average crust thicknesses for Nameless, Unicorn, and MTR seamounts.

water depth limit should be maintained because Cu is of limited economic potential either below or above the 2,500 m water depth and because the most economically important Fe-hosted metal –Te – does not show increasing concentrations with depth. In addition, most resource studies for the Pacific consider the 2,400–2,500 m isobath as the depth limit for calculations, and so comparisons of our data with Pacific data would not be valid using a different water depth limit.

We consider the following: (i) a large area represented by MTR (total surface area of 41,872 km^2); (ii) a medium-sized area, represented by the combined areas of Lion, Nameless, Dragon, and Unicorn Seamounts (total surface area of 7,824 km^2); and (iii) a small area represented by the combined areas of Lion and Nameless seamounts (total surface area of 3,676 km^2) (Figure 9). The choice of Nameless, Lion, Dragon, and Unicorn seamounts was made because we expect that these seamounts located to the south of MTR may represent a suitable exploration area based on their depths, specific oceanic currents, and metal concentrations. Area calculations and reductions for the three scenarios are illustrated in Figure 10.

Hein et al. (2009) calculated surface areas for two case studies: (i) a large guyot (total surface area of 11,761 km^2) and (ii) an average-size guyot (total surface area of 3,495 km^2). Considering the worst-case scenario (50% reduction of crust-covered surface above 2,500 m water depth due to topographic and biological limitations for initial 60% sediment cover reduction), Hein et al. (2009) obtained, respectively, 615 km^2 and

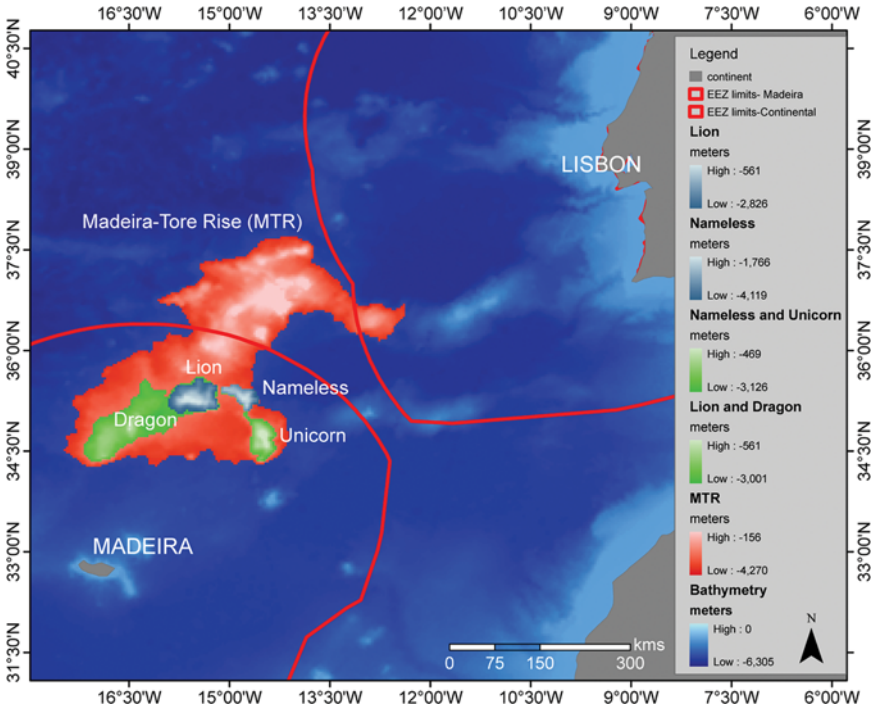

Figure 9. Madeira-Tore Rise; Lion and Dragon, and Nameless and Unicorn; and Lion and Nameless contour polygons used for surface area calculations. (Color figure available online.)

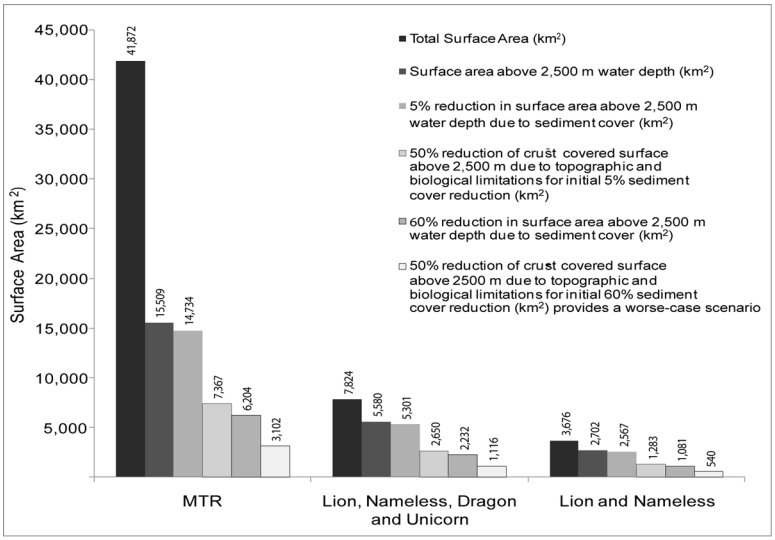

Figure 10. Histogram of total surface area and surface area above 2,500 m water depth for the three scenarios that consider different sizes of seamount areas. Other bars represent reductions in size of areas where crusts might be available because of sediment cover and other considerations (see Hein et al. 2009).

231 km^2 of permissible area. A worst-case scenario for our dataset would yield surface areas of 3,102, 1,116, and 540 km^2, for the three groups described above, respectively (Figure 10). Considering these surface areas, a wet bulk density of 1.95 g/cm^3, an annual production of 1 million tons, and assuming a general mean crust thickness of 3 cm rather than using the limited dataset that we have for crust thicknesses from each seamount, the area needed to maintain a 20-year mine site is 342 km^2, which can be potentially accommodated by all three groups. These results are comparable to the results obtained by Hein et al. (2009) for central equatorial Pacific seamounts.

We also calculated metal tonnages considering the above conditions (worst-case scenario and 3 cm mean crust thickness). The metal concentrations used for these calculations are the ones given previously. We also calculated the dry-tonnages using a mean dry-bulk density of crusts of 1.3 g/cm^3 (Hein et al. 2000). In Figure 11 we

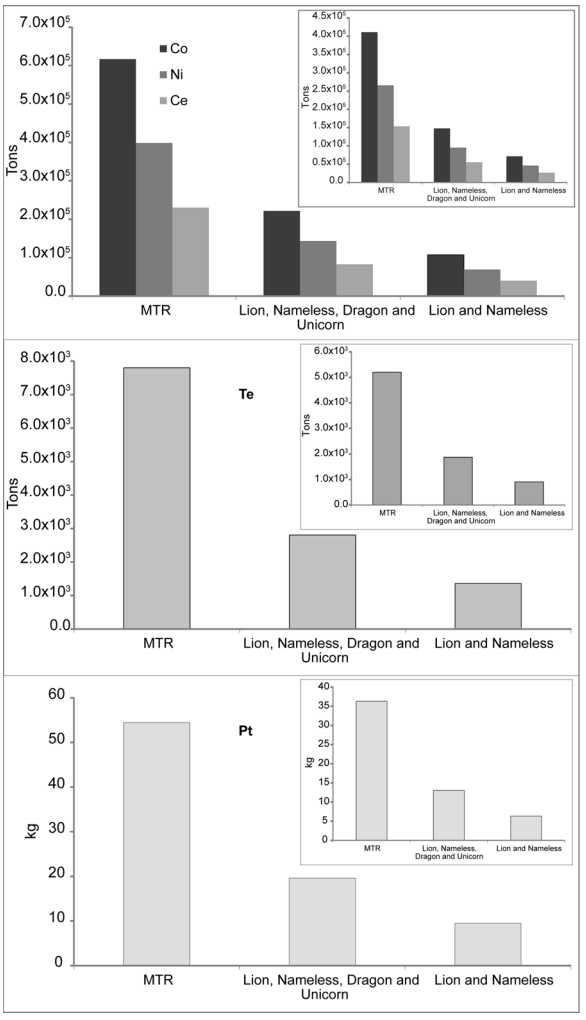

Figure 11. Histogram of calculated tonnages (wet weight) for different metals considering the worst-case scenario of surface area reductions. Insets plots show areas corresponding to calculated tonnages based on dry weight.

present a histogram of calculated tonnages (wet- and dry-weight) for the metals considered. Maximum tonnages (resulting from large area calculations) for Co, Ni, Ce, Te and Pt are 6.2×10^5, 4.0×10^5, 2.3×10^5, 7.8×10^3 and 5.4×10^{-2} tons, respectively. Considering the small area, our calculations result in 1.1×10^5, 6.9×10^4, 4.0×10^4, 1.4×10^3 and 9.5×10^{-3} tons for the same metals, respectively. Our results show that the study area within the Portuguese EEZ (and adjacent areas in International Waters, for MTR; Figure 11) is comparable to that of areas in the central Pacific Ocean presented in Hein et al. (2009). Exploration beyond reconnaissance may now be warranted and should include detailed sampling, backscatter side-scan sonar, bathymetric mapping, and detailed mapping of crust thicknesses, etc., in order to better constrain the assumptions made here and to allow for a quantitative resource evaluation.

Conclusions

The objective of this study was to determine the composition of Fe-Mn crusts from the northeast Atlantic and to consider gaps in our knowledge needed for assessing the quantitative resource potential of these deposits. The compositions of the studied crusts are typical for hydrogenetic crusts adjacent to continental margins. Specific compositional differences are found that likely indicate specific local conditions during crust accretion, for example higher Co, Ni, and Zr in Pacific crusts and higher Th in Atlantic crusts.

The enrichment of trace metals of economic interest in Fe-Mn crusts is of particular importance for their potential as a resource (i.e., Te and REEs), and is of specific interest for the resource potential of these deposits within the Portuguese EEZ. Based on the criteria of Hein et al. (2009), we calculated tonnages for specific metals in chosen areas in and adjacent to the Portuguese EEZ. Our results indicate that the study area is comparable to parts of the central Pacific Ocean and may represent an important metal resource for the future. Further studies are warranted in order to better constrain and quantify the results presented here.

References

Amante, C. and B. W. Eakins. 2009. *ETOPO1 1 Arc-Minute Global Relief Model: Procedures, Data Sources and Analysis.* Vol. March 2009, *NOAA Technical Memorandum NESDIS NGDC-24*.

Ambar, I., L. Armi, A. Bower, and T. Ferreira. 1999. Some aspects of time variability of the Mediterranean Water off south Portugal. *Deep-Sea Research I* 46: 1109–1136.

Ambar, I. and M. R. Howe. 1979. Observations of the Mediterranean outflow-I Mixing in the Mediterranean Outflow. *Deep-Sea Research I* 26A: 535–554.

Ambar, I., N. Serra, M. J. Brogueira, G. Cabeçadas, F. Abrantes, P. Freitas, C. Gonçalves, and N. Gonzalez. 2002. Physical, chemical and sedimentological aspects of the Mediterranean outflow off Iberia. *Deep-Sea Research II* 49: 4163–4177.

Anders, E. and N. Grevesse. 1989. Abundances of the elements: Meteoritic and solar. *Geochimica et Cosmochimica Acta* 53: 197–214.

Banakar, V. K., J. R. Hein, R. P. Rajani, and A. R. Chodankar. 2007. Platinum group elements and gold in ferromanganese crusts from Afanasiy-Nikitin seamount, equatorial Indian Ocean: Sources and fractionation. *Journal of Earth System Science* 116: 3–13.

Bau, M., A. Koschinsky, P. Dulski, and J. R. Hein. 1996. Comparison of the partitioning behaviors of yttrium, rare-earth elements, and titanium between hydrogenetic marine ferromanganese crusts and seawater. *Geochimica et Cosmochimica Acta* 60: 1709–1725.

Broecker, W. S. and T.-H. Peng. 1982. *Tracers in the Sea*. Palisades, New York: Lamont-Doherty Geological Observatory, Columbia University.

Bruland, K. W., E. L. Rue, and G. J. Smith. 2001. Iron and macronutrients in California coastal upwelling regimes: Implications for diatom blooms. *Limnology and Oceanography* 46: 1661–1674.

Burns, R. G. and V. M. Burns. 1977. Mineralogy. In: *Marine Manganese Deposits*. Glasby, G. P. (ed.), 185–248. Amsterdam: Elsevier.

Cook, H. E., P. D. Johnson, J. C. Matti, and I. Zemmels. 1975. Methods of sample preparation and X-ray data analysis (X-ray mineralogy laboratory, Deep Sea Drilling Project, University of California Riverside). *In Initial Reports of the Deep-Sea Drilling Project* 28: 999–1007.

Craig, J. D., J. E. Andrews, and M. A. Meylan. 1982. Ferromanganese Deposits in the Hawaiian Archipelago. *Marine Geology* 45: 127–157.

Cronan, D. S. 1977. Deep-sea nodules: distribution and geochemistry. In: *Marine Manganese Deposits*. Glasby, G. P. (ed.), 11–44. Amsterdam: Elsevier.

———. 1997. Some controls on the geochemical variability of manganese nodules with particular reference to the tropical South Pacific. In: *Manganese Mineralization: Geochemistry and mineralogy of terrestrial and marine deposits, Geological Society Special Publication 119*. Nicholson, K., Hein, J. R., Buhn, J. R. and Dasgupta, S. (eds.), 139–151. Bath, U.K.: The Geological Society.

De Carlo, E. H. 1991. Paleoceanographic implications of rare earth element variability within a Fe-Mn crust from the central Pacific Ocean. *Marine Geology* 98: 449–467.

Elderfield, H., C. J. Hawkesworth, M. J. Greaves, and S. E. Calvert. 1981. Rare earth element geochemistry of oceanic ferromanganese nodules and associated sediments. *Geochimica et Cosmochimica Acta* 45: 513–528.

Frank, M., R. K. O'Nions, J. R. Hein, and V. K. Banakar. 1999. 60 Ma records of major elements and Pb-Nd isotopes from hydrogenous ferromanganese crusts: Reconstruction of seawater paleochemistry. *Geochimica Cosmochimica Acta* 63: 1689–1708.

Gaspar, L. 2001. Química e mineralogia de depósitos de ferromanganês da montanha submarina Lion, ZEE da Madeira, Portugal. Paper read at Actas do VI Congresso de Geoquímica dos Países de Língua Portuguesa/XII Semana da Geoquímica, at Faro, Portugal, April 9–12.

Geldmacher, J., K. Hoernle, A. Klugel, P. V. D. Bogaard, F. Wombacher, and B. Berning. 2006. Origin and geochemical evolution of the Madeira-Tore Rise (eastern North Atlantic). *Journal of Geophysical Research* 111: B09206, doi: 10.1029/2005JB003931.

Goldberg, E. D., M. Koide, R. A. Schmitt, and R. H. Smith. 1963. Rare earth distribution in the marine environment. *Journal of Geophysical Research* 68: 4209–4217.

Halbach, P., E. Rehm, and V. Marchig. 1979. Distribution of Si, Mn, Ge, Ni, Cu, Co, Zn, Pb, Mg, and Ca in Grain-Size Fractions of Sediment Samples from a Manganese Nodule Field in the Central Pacific Ocean. *Marine Geology* 29: 237–252.

Halbach, P. 1986. Process controlling the heavy metal distribution in Pacific ferromanganese nodules and crusts. *Geologische Rundschau* 75: 235–247.

Halbach, P., F. T. Manhein, and P. Otten. 1982. Co-rich ferromanganese deposits in the marginal seamount regions of the central Pacific basin: results of the Midpac'81. *Erzmetall* 35: 447–453.

Halbach, P., C. Kriete, B. Prause, and D. Puteanus. 1989a. Mechanisms to explain the platinum concentration in ferromanganese seamount crusts. *Chemical Geology* 76: 95–106.

Halbach, P. E., C-D. Sattler, F. Teichmann, and M. Washner. 1989b. Cobalt-rich and platinum-bearing manganese crust deposits on seamounts: nature, formation, and metal potential. *Marine Mining* 8: 23–39.

Halbach, P., B. Prause, K. Koch, and M. Westholt. 1990. Platinum and Palladium in Co-Rich Ferromanganese Crust Deposits. *Marine Mining* 9: 117–126.

Halbach, P. and Scientific Crew. 1993. Marine geological and geochemical investigations of sediments, precipitates and hard rocks from three seamounts in the NE Atlantic to identify element fluxes. *Technical cruise report of the RV Sonne cruise SO 83 – MARFLUX 4; BMFT project 03R424A6 and MAST contract 0022C*. Berlin, Germany: Freie Universitat Berlin.

Hein, J. R. 2004. Cobalt-rich ferromanganese crusts: Global distribution, composition, origin and research activities. *Minerals other than Polymetallic nodules of the International Seabed Area. Proceedings of a Workshop held on 26–30 June 2000*, 188–256. Kingston, Jamaica: International Seabed Authority.

Hein, J. R., T. A. Conrad, and R. E. Dunham. 2009. Seamount Characteristics and Mine-Site Model Applied to Exploration- and Mining-Lease-Block Selection for Cobalt-Rich Ferromanganese Crusts. *Marine Georesources and Geotechnology* 27: 160–176. doi: 10.1080/10641190902852485.

Hein, J. R., T. A. Conrad, and H. Staudigel. 2010. Seamount Mineral Deposits, a source of rare metals for high-technology industries. *Oceanography* 23(1): 184–189.

Hein, J. R., A. Koschinsky, M. Bau, F. T. Manheim, J.-K. Kang, and L. Roberts. 2000. Cobalt-Rich ferromanganese crusts in the Pacific. In: *Handbook of Marine Mineral Deposits*. Cronan, D. S. (ed.), 239–279. Boca Raton, Florida: CRC Press.

Hein, J. R., A. Koschinsky, P. Halbach, F. T. Manheim, M. Bau, J-K. Kang, and N. Lubick. 1997. Iron and manganese oxide mineralization in the Pacific. In: *Manganese Mineralization: Geochemistry and mineralogy of terrestrial and marine deposits, Geological Society Special Publication 119*. Nicholson, K., Hein, J. R., Buhn, J. R. and Dasgupta, S. (eds.), 123–138. Bath, U.K.: The Geological Society.

Hein, J. R., A. Koschinsky, and A. N. Halliday. 2003. Global occurrence of tellurium-rich ferromanganese crusts and a model for the enrichment of tellurium. *Geochimica et Cosmochimica Acta* 67(6): 1117–1127.

Hein, J. R., A. Koschinsky, and B. McIntyre. 2005. The global enrichment of platinum group elements in marine ferromanganese crusts. *Extended Abstracts, 10th International Platinum Symposion*. Tórmánen, T. O. and Alapeti, T. T. (eds.), 7–11 August 2005, Oulu, Finland, 98–101.

Hein, J. R., W. C. Schwab, and A. S. Davis. 1988. Co and Pt-rich ferromanganese crusts and associated substrate rocks from the Marshall Islands. *Marine Geology* 78: 255–283.

Hein, J. R., H.-W. Yeh, S. H. Gunn, W. V. Sliter, L. M. Benninger, and C.-H. Wang. 1993. Two major Cenozoic episodes of phosphogenesis recorded in Equatorial Pacific seamount deposits. *Paleoceanography* 8(2): 293–311.

Hodge, V. F., M. Stallard, M. Koide, and E. D. Goldberg. 1985. Platinum and the platinum anomaly in the marine environment. *Earth and Planetary Science Letters* 72: 158–162.

Hoernle, K. and Scientific Party. 2003. Cruise Report M51/1. In: *Ostatlantik – Mittelmeer – Schwarzes Meer, Cruise No. 51*, 12 September–28 December 2001, Meteor-Berichte 03-1. C. Hemleben, K. Hoernle, B. B. Jorgensen and W. Roether (eds.). Hamburg, Germany: University of Hamburg.

Intergovernmental Oceanographic Commission (IOC). 2002. Geological Processes in the Mediterranean and Black Seas and North East Atlantic. Preliminary results of investigations during the TTR-11 cruise of RV Professor Logachev, July-September, 2001. *IOC Technical Series*, N. H. Kenyon, M. K. Ivanov, A. M. Akhmetzhanov and G. G. Akhmanov (eds.), Paris, France: UNESCO.

Jones, E. J. W., M. K. BouDagher-Fadel, and M. F. Thirlwall. 2002. An investigation of seamount phosphorites in the Eastern Equatorial Atlantic. *Marine Geology* 183: 143–162.

Klovan, J. E. and J. Imbrie. 1971. An algorithm and FORTRAN-IV program for large-scale Q-mode factor analysis and calculation of factor scores. *Mathematical Geology* 3: 61–77.

Koschinsky, A. and P. Halbach. 1995. Sequential leaching of marine ferromanganese precipitates: Genetic implications. *Geochimica et Cosmochimica Acta* 59: 5113–5132.

Koschinsky, A., P. Halbach, J. R. Hein, and A. Mangini. 1996. Ferromanganese crusts as indicators for paleoceanographic events in the NE Atlantic. *Geologische Rundschau* 85: 567–576.

Koschinsky, A., M. van Gerven, and P. Halbach. 1995. First investigations of massive ferromanganese crusts in the NE Atlantic in comparison with hydrogenetic Pacific occurrences. *Marine Georesources and Geotechnology* 13: 375–391.

Koschinsky, A., A. Stascheit, M. Bau, and P. Halbach. 1997. Effects of phosphatization on the geochemical and mineralogical composition of marine ferromanganese crusts. *Geochimica et Cosmochimica Acta* 61(19): 4079–4094.

Kuhn, T., M. Bau, N. Blum, and P. Halbach. 1998. Origin of negative Ce anomalies in mixed hydrothermal-hydrogenetic Fe-Mn crusts from the Central Indian Ridge. *Earth and Planetary Science Letters* 163: 207–220.

Madelain, F. 1970. Influence de la topographie du fond sur l'écoulement Mediterranéen entre le Détroit de Gibraltar et le cap Saint-Vincent. *Cahiers Océanographiques* 22: 43–61.

Mangini, A., P. Halbach, D. Puteanus, and M. Segl. 1987. Chemistry and Growth of Central Pacific Mn-Crusts and Their Economic Importance. In: *Marine Minerals, Advances in Research and Resource Assessment*. Teleki, P. G., Dobson, M. R., Moore, J. R. and Stackelberg, U. V. (eds.), 205–220. Dordrecht Germany: D Reidel Publishing Company.

Merle, R. 2006. Age and origin of Tore-Madeira Rise: beginning of Atlantic Ocean spreading or hotspot track. Petrology, geochemistry, U-Pb geochronology and Pb-Sr-Hf isotopes. PhD Thesis. University of Nantes, Nantes, (in French).

Merle, R., U. Schärer, J. Girardeau, and G. Cornen. 2006. Cretaceous seamounts along the continent-ocean transition of the Iberian margin: U-Pb ages and Pb-Sr-Hf isotopes. *Geochimica et Cosmochimica Acta* 70(19): 4950–4976.

Moffet, J. W. 1994. A radiotracer study of cerium and manganese uptake onto suspended particles in Chesapeake Bay. *Geochimica et Cosmochimica Acta* 58: 695–703.

Muiños, S. B. 2005. Contribuição da análise multivariada para o estudo de crostas submarinas de ferro e manganês do Atlântico Nordeste. Master, Instituto Superior Técnico, Lisbon, Portugal: Universidade Técnica de Lisboa, (in Portuguese).

Muiños, S. B., L. Gaspar, J. H. Monteiro, R. Salgueiro, J. F. Ramos, V. H. Magalhães, and T. Rodrigues. 2002. Ferromanganese deposits from the Nameless Seamount: Preliminary results. *IOC Workshop Report* 183: 27–30.

Nath, B. N., V. Balaram, M. Sudhakar, and E. W. L. Plueger. 1992. Rare-earth element geochemistry of ferromanganese deposits from the Indian Ocean. *Marine Chemistry* 38: 185–208.

Pereira, H. G., S. Renca, and J. Saraiva. 2003. A case study on geochemical anomaly identification through principal components analysis supplementary projection. *Applied Geochemistry* 18: 37–44.

Sholkovitz, E. R. and D. L. Schneider. 1991. Cerium redox cycles and rare earth elements in the Sargasso Sea. *Geochimica et Cosmochimica Acta* 55: 2737–2743.

Taylor, S. R. and S. M. McLennan. 1985. *The Continental Crust: Its Composition and Evolution*. Oxford: Blackwell.

Usui, A., T. A. Mellin, M. Nohara, and M. Yuasa. 1989. Structural stability of marine 10A manganates from the Ogasawara (Bonin) arc: Implication for low-temperature hydrothermal activity. *Marine Geology* 86: 41–56.

van Andel, T. H. 1975. Mesozoic-Cenozoic calcite compensation depth and the global distribution of calcareous sediments. *Earth and Planetary Science Letters* 21: 455–480.

Varentsov, I. M., V. A. Drits, A. I. Gorshkov, A. V. Sivtsov, and B. A. Sakharov. 1991. Mn-Fe oxyhydroxide crusts from the Krylov seamount (eastern Atlantic): Mineralogy, Geochemistry and Genesis. *Marine Geology* 96: 53–70.

Verlaan, P. A., D. S. Cronan, and C. L. Morgan. 2004. A comparative analysis of compositional variations in and between marine ferromanganese nodules and crusts in the South Pacific and their environmental controls. *Progress in Oceanography* 63: 125–158.

von Stackelberg, U., H. Kuzendorf, V. Marchig, and R. Gwodz. 1984. Growth history of a large ferromanganese crust from the equatorial North Pacific nodule belt. *Geologisches Jahrbuch* A75: 213–235.

Vonderhaar, D. L., G. M. McMurty, D. Garbe-Schónberg, D. Stüben, and B. K. Esser. 2000. Platinum and other related element enrichment in Pacific ferromanganese crust deposits. In: *Marine authigenesis: From global to microbial, SEPM Special Publication 66*. Glenn, C. R., Prévôt-Lucas, L. and Lucas, J. (eds.), 287–308. Tulsa, Oklahoma: SEPM.

Wen, X., E. H. De Carlo, and Y. H. Li. 1997. Interelement relationships in ferromanganese crusts from the central Pacific ocean: their implications for crust genesis. *Marine Geology* 136: 277–297.

Zenk, W. 1970. On the temperature and salinity structure of the Mediterranean Water in the Northeast Atlantic. *Deep-Sea Research* 17: 627–631.